ATM inhibition augments type I interferon response and antitumor T-cell immunity when combined with radiation therapy in murine tumor models

Won Jong Jin [ID],[1] Luke M Zangl,[1] Meredith Hyun,[2] Elian Massoud,[1] Kaleb Schroeder,[1] Roxana A Alexandridis,[2] Zachary S Morris [ID] [1]

[1]Department Human Oncology, University of Wisconsin-Madison, Madison, Wisconsin, USA
[2]Department of Biostatistics and Medical Informatics, University of Wisconsin-Madison, Madison, Wisconsin, USA

Correspondence to
Dr Zachary S Morris;
zmorris@humonc.wisc.edu

ABSTRACT

Background Radiation therapy (RT) elicits DNA double-strand breaks, resulting in tumor cytotoxicity and a type I interferon (IFN) response via stimulator of interferon genes (STING) activation. We investigated whether combining RT with an ataxia-telangiectasia mutated inhibitor promoted these effects and amplified tumor immunity.

Methods Mice-bearing syngeneic flank tumors (MOC2 head and neck squamous cell carcinoma or B78 melanoma) were treated with tumor-directed RT and oral administration of AZD0156. Specific immune cell depletion, type 1 interferon receptor 1 knock-out mice (IFNAR1-KO), and STING-deficient tumor cells were used to investigate tumor-immune crosstalk following RT and AZD0156 treatment.

Results Combining RT and AZD0156 reduced tumor growth compared with RT or AZD0156 alone in mice bearing MOC2 or B78 tumors. Low-dose AZD0156 (1–100 nM) alone did not affect tumor cell proliferation but suppressed tumor cell clonogenicity in combination with RT. Low-dose AZD0156 with RT synergistically increased IFN-β, major histocompatibility complex (MHC)-I, and programmed death-ligand 1 (PD-L1) expression in tumor cells. In contrast to wild-type mice, IFNAR1-KO mice showed reduced CD8+T cell tumor infiltration and poor survival following RT+AZD0156 treatment. CD8+T cell depletion reduced antitumor response during RT+AZD0156 treatment. STING-deficient MOC2 (MOC2-STING+/−) or B78 (B78-STING−/−) tumors eliminated the effects of RT+AZD0156 on the expression of IFN-β, MHC-I, and PD-L1, and reduced CD8+T cell infiltration and migration. Additional anti-PD-L1 therapy promoted antitumor response by elevation of tumor-MHC-I and lymphocyte activation.

Conclusions Combined radiation and AZD0156 increase STING-dependent antitumor response. Tumor-derived cell-autonomous IFN-β amplification drives both MHC-I and PD-L1 induction at the tumor cell surface, which is required by anti-PD-L1 therapy to promote antitumor immune response following RT and AZD0156 combination therapy.

INTRODUCTION

Radiation therapy (RT) can induce DNA double-strand breaks (DSBs) in cells,

WHAT IS ALREADY KNOWN ON THIS TOPIC

⇒ Ataxia-telangiectasia mutated (ATM) inhibition contributes to blocking DNA-damage repair, resulting in tumor death and stimulator of interferon genes (STING)-dependent and independent type I interferon (IFN) induction.

WHAT THIS STUDY ADDS

⇒ The ATM inhibitor, AZD0156, synergistically induces STING-dependent type I IFN expression in radiated MOC2 head and neck cell carcinoma and B78 melanoma and increases CD8+T cell migration and infiltration. IFN-β derived from tumor-STING activation stimulates major histocompatibility complex I and programmed death-ligand 1 (PD-L1) expression in tumors. Addition of anti-PD-L1 therapy improves antitumor response and lymphocyte activation following radiation therapy combined with ATM inhibitor.

HOW THIS STUDY MIGHT AFFECT RESEARCH, PRACTICE OR POLICY

⇒ Combined ATM inhibitor and tumor radiation therapy elicit an antitumor immune response but require anti-PD-L1 treatment to prevent immune exhaustion. This provides a therapeutic strategy for targeting tumors that are poorly immunogenic or those that are poorly responsive to radiotherapy.

resulting in the induction of cytoplasmic double stranded DNA (dsDNA) and cytotoxicity. While RT can confer direct tumor killing effects, it can also interact with the immune system to stimulate tumor antigen presentation and expression of immune susceptibility factors.[1 2] Among these tumor phenotypical changes, the stimulator of interferon genes (STING) pathway plays a crucial role in intrinsic type 1 interferon (IFN-I) expression in tumor cells following RT.[3 4] A previous study has shown that intratumoral IFN-I expression selectively expands antigen-specific T cells,

enhancing an antitumor response.[2] In contrast, systemic IFN-I therapy showed severe side effects, inflammation, and tissue cytotoxicity.[5] Therefore, local tumor RT may be an effective approach to locally inducing IFN-I in tumors, and this has the potential to enhance the efficacy of other immunotherapies, particularly in the setting of poorly immunogenic tumors that may not respond to immunotherapy alone.

While RT alone may enable local tumor control, it is generally not effective in modifying the risk for systemic disease that is not directly targeted by RT. Preclinical and clinical data demonstrate multiple immunogenic effects of RT, ultimately leading to diversification of antitumor T-cell response and enhanced response to immune checkpoint inhibitors.[6 7] This has led to tremendous interest in combining RT with immunotherapies such as an immune checkpoint inhibitor for the purpose of enhancing the systemic antitumor immune response, particularly in poorly immunogenic tumors that are unlikely to respond to immune checkpoint blockade alone. Preclinical and clinical studies show that RT can safely be delivered in combination with immune checkpoint blockade and these studies demonstrate detectable local and sometimes systemic effects of focal RT on antitumor immunity.[7–12] However, clinical studies to date have not yet conclusively demonstrated that RT can increase the rate or depth of response to immune checkpoint inhibition.[7 13 14] This may suggest a need and opportunity for further boosting or modulating the immunogenic effects of RT to better stimulate antigen presentation and/or IFN-I response to elicit a more potent antitumor immune response.

While RT triggers STING-mediated IFN-I signaling activation, DNA damage response (DDR) detects DNA-DSBs and initiates DNA repair.[15] In the DDR process, ataxia-telangiectasia mutated (ATM) is known to have a critical role in response to DNA-DSB, and in this context it elicits cell cycle arrest that enables cell survival and genomic stability.[16 17] On DNA-DSB, ATM phosphorylates histone H2A variant H2AX (γH2AX) to recruit DDR molecular machinery to the DSB sites, enabling DNA repair initiation.[18] Because of these functions, ATM inhibition has been suggested as a mechanism for sensitizing tumor cells to the damage from RT.[19 20] In preclinical studies, the selective ATM inhibitor AZD0156 replicated a DDR-deficient phenotype in human FaDu head and neck cell carcinoma (HNSCC) and appeared to impede DNA damage repair, resulting in greater tumor cell apoptosis when combined with a poly (ADP-ribose) polymerase 1 (PARP) inhibitor.[21] In addition to these tumor-killing effects, another ATM inhibitor KU60019 showed activation of IFN-I in pancreatic tumor cells via an STING-independent manner.[22] More recently, ATM-knockout (KO) in murine B16F10 melanoma was observed to result in tumor growth inhibition that was dependent on the Cyclic GMP–AMP synthase (cGAS)/STING pathway.[23] In addition, ATM inhibition on irradiated tumor cells showed mitotic disruption, STING pathway activation, and programmed death-ligand 1 (PD-L1) expression in tumors.[24] Furthermore, another

group reported that combined radiation and ATM inhibition showed increased CD8+T cell infiltration, decreased CD4+T cell infiltration, and PD-L1 induction in tumor-associated macrophages.[25] These previous reports suggest a capacity for ATM inhibition to modulate the immunogenic effects of radiation within the tumor microenvironment, however further investigation is needed to clarify the mechanisms of this interaction.

Although both RT and ATM inhibition can activate a STING-dependent IFN-I response in tumor cells, the effect of combined treatment with RT and ATM inhibition on IFN-I response and antitumor immunity has not been fully elucidated. In the present study, we evaluate the use of AZD0156 in combination with RT for poorly immunogenic syngeneic murine tumor models of HNSCC and melanoma. AZD0156 is an orally bioavailable ATM inhibitor that has been under early phase clinical investigation (NCT02588105). Here, we report that a combination of AZD0156 and local tumor RT augments the antitumor immune response. Our results provide a rationale for further evaluating the therapeutic potential of combining RT and ATM inhibition in combination with immunotherapies.

MATERIALS AND METHODS
Cell lines
The murine HNSCC cell line MOC2 was obtained from Ravindra Uppaluri (Brigham and Women's Hospital and Dana-Farber Cancer Institute) and the murine melanoma cell line B78-D14 (B78) was obtained from Ralph Reisfeld (Scripps Research Institute). The MOC2 HNSCC model displays a high level of regulatory T-cell infiltration and is poorly responsive to immune checkpoint inhibition.[26 27] The B78 melanoma model exhibits little baseline expression of major histocompatibility complex (MHC)-I, limited lymphocyte infiltration of tumors, and is also poorly responsive to immune checkpoint inhibition alone.[28] The MOC2 cells were cultured using Dulbecco's Modified Eagle Medium (DMEM; Corning)/Ham's F12 (Corning) at a 2:1 mixture containing 5 ng/mL epidermal growth factor (Gibco), 400 ng/mL hydrocortisone (Sigma-Aldrich), and 5 µg/ mL insulin (Sigma-Aldrich), 1% penicillin/streptomycin (Life Technologies), and 5% fetal bovine serum (FBS, Life Technologies). The B78 cells were cultured with RPMI-1640 containing 10% of FBS and 1% penicillin/streptomycin (Life Technologies). The human HNSCC cell line SCC6 was cultured in DMEM containing 10% FBS, 1 mg/mL hydrocortisone, and 1% penicillin/streptomycin. All cells were incubated in a humidified incubator at 37°C in an atmosphere of 5% carbon dioxide. American Type Culture Collection (ATCC) guidelines were followed for cell line authentication by monitoring morphology, growth curve, and *Mycoplasma* testing[29]

Tumor models
Mice were housed and treated in accordance with the Guide for Care and Use of Laboratory Mice. Treatments

were performed under a protocol (protocol number M005670) approved by the University of Wisconsin Institutional Animal Care and Use Committee. Female C57BL/6 mice aged 6–8 weeks were purchased from Taconic. Female B6(Cg)-Ifnar1$^{tm1.2Ees}$/J mice (type I interferon receptor 1 knockout (IFNAR1-KO)) were purchased from The Jackson Laboratory.

The B78 and MOC2 cells were engrafted through subcutaneous flank injection of 2×10^6 cells into the right flank (for single tumor-bearing models) or right and left flanks (bilateral tumor-bearing models). Tumor sizes were determined using digital calipers, and tumor volumes were approximated as (width^2×length)/2. Mice were randomized at a mean tumor volume reaching 150–200 mm^3, about 10 days after MOC2 or 28 days after B78 implantation. The initial treatment day was defined as "day 1" for all in vivo experiments, including tumor growth and mouse survival. Tumor growth was measured until day 30–42 after treatment initiation, and the probability of mouse survival was tracked until day 60–70. Experiment endpoint/euthanasia of mice criteria included tumor diameter >20 mm or hunched posture.

Treatments
RT in vivo was conducted using a cabinet orthovoltage X-ray biological irradiator, X-RAD 320 (Precision X-Ray). Local tumor RT was delivered to the exposed tumor by shielding the rest of the mouse using custom lead jigs. RT in vitro was performed using a Cell Irradiator RS225 (Xstrahl), and radiation delivery to the cells was performed at least 24 hours after cell culture. ATM inhibitor compound AZD0156 was obtained from AstraZeneca. AZD0156 was dissolved in 100% dimethyl sulfoxide (DMSO, Sigma-Aldrich) for in vitro or corn oil 90% (Sigma-Aldrich) + 10% DMSO for in vivo. AZD0156 (10 mg/kg) was given orally 1 hour before tumor irradiation and administered once per day for five consecutive days. Anti-IgG2b (Bio X Cell) or anti-PD-L1 (clone B7-H1, Bio X Cell) antibody (200 µg) was given via intraperitoneal injection on days 0, 4, 8, and 12.

Flow cytometry
Sample preparation for the flow cytometry was performed as previously described.[30] Briefly, tumors were collected and dissociated using a Miltenyi gentle-MACS Octo Dissociator in RPMI-1640 (Corning) containing DNase (500 µg, Sigma-Aldrich) and collagenase (5 mg, Sigma-Aldrich) for 30 min. Peripheral blood mononuclear cells (PBMCs) were collected from the submandibular vein. Spleens were extruded and splenocytes isolated using a plunger to filter these through a 70 µm strainer. Obtained tumor dissociates, PBMCs, and splenocytes were incubated with red blood cell (RBC) lysis buffer (BioLegend) and filtered through a 70 µm strainer in the presence of RPMI-1640.

The single-cell suspensions were subjected to live/dead cell staining using Ghost Red Dye 780 (Tonbo Biosciences). Then, external antigens were labeled using a flow cytometry detectible antibody. Internal antigens were labeled using BD Cytofix/Cytoperm according to the manufacturer's instructions. Flow cytometry analysis was optimized by bead compensation (UltraComp eBeads, Invitrogen) and followed fluorescence minus one gating methodology. Attune NxT Flow Cytometer (Thermo Fisher) was used for flow cytometry, and FlowJo Software (TreeStar) was used for the data analysis. The following antibodies were used for flow cytometry analysis. PE/Cyanine7 anti-CD45 (13/2.3), FITC anti-CD3 (17A2), BV510 anti-CD4 (RM4-5), PerCP/Cyanine5.5 anti-CD8a (53–6.7), BV605 anti-NK1.1 (PK136), BV421 anti-CD69 (H1.2F3), PE anti-GZMB (QA16A02), FITC anti-MHC I (H-2, M1/42), BV711 anti-CD44 (clone# IM7), BV510 anti-CD62L (clone# MEL-14), Alexa Fluor 700 anti-CD62L (clone# MEL-14), BV711 anti-TNF-α (clone# MP6-XT22), APC anti-IFN-γ (clone# XMG1.2), and APC anti-γH2AX (clone# 2F3).

Western blot
Tumor cells (5×10^5 cells / well) were cultured in a 6-well plate for 24 hours. Then the tumor cells were radiated 1 hour after treatment with DMSO or AZD0156 (50 nM). The treated cells were collected, lysed and western blot was performed as previously described with minor modification.[10] Briefly, cells were lysed using a radioimmunoprecipitation assay (RIPA) buffer (Thermo Scientific) containing protease inhibitor cocktail (Thermo Scientific). Proteins were quantified using Pierce BCA Protein Assay (Thermo Scientific). 30 µg of lysates were heat-denatured and loaded in a gradient gel (4–20%, Bio-Rad). Then the proteins in the gel were transferred to a polyvinylidene fluoride (PVDF) membrane (Millipore) for 2 hours at 4°C at 50 V constant voltage. The membrane was probed with primary antibodies, γH2AX (Ser 139, clone 20E3), STING (clone D2P2F), and β-actin (clone 13E5) at 4°C overnight. Then, the membrane was labeled with a horseradish peroxidase (HRP)-conjugated goat anti-rabbit IgG secondary antibody (Bio-Rad) at room temperature for 1.5 hours. Chemiluminescent substrate (Azure Biosystem) was used to visualize the protein band, and pictures were obtained using Azure Biosystem (C600). A Prestained Protein Ladder (Thermo Scientific) was used to estimate molecular weight.

Cell viability assay
Tumor cells (1×10^3 cells/well) were plated in a 96-well plate. After 24 hours, the culture media were exchanged in the presence of a varied concentration of AZD0156 or DMSO control. The cells were further incubated at the indicated time points. Viable cells were measured using the Cell Counter Kit 8 (Enzo Life Sciences) according to the manufacturer's instructions. Absorbance was measured at 450 nm using SpectraMax i3 (Molecular Devices).

Clonogenic assay

Tumor cells (5×10^5 cells/well) were cultured in a 6-well plate for 24 hours to allow the cells to adhere. Monolayer cells were radiated with either 0, 4, 8, or 12 Gy. After RT, the cells were replated in the presence of DMSO or AZD0156 (50 nM) and cultured until colony formation in the 0 Gy control group. Then, the cells were washed with phosphate buffered saline twice and stained using 0.5% crystal violet containing methanol. Colonies consisting of 20 or more cells were scored, and the surviving fraction was determined as the (number of colonies)/(number of plated cells×plating efficiency). The log surviving fraction of each group was calculated and plotted.

Cytoplasmic double stranded DNA measurement

Live cell number was determined using auto cell counter Countess 3 (Invitrogen) after trypan blue staining (HyClone). Then, the cytoplasmic extracts were isolated by NE-PER Nuclear and Cytoplasmic Extraction Reagents (Thermo Scientific). The amount of dsDNA in the cytoplasmic extracts was measured using QuantiFluor ONE dsDNA System (Promega) and SpectraMax i3 (Molecular Devices).

T-cell sorting and activity evaluation

Spleens collected from mice were mechanically digested using a plunger and filtered through a 70 μm strainer in RPMI-1640 (4 mL). The single-cell suspension was centrifuged at 2000 rpm for 10 min at 4°C, subjected to RBC lysis, then filtered through a 70 μm strainer again. Prepared single-cell suspensions were used to sort CD8+T cells using a magnetic-activated cell sorting (MACS)-negative selection kit (Miltenyi Biotec). Sorted CD8+T cells (2×10^5) were cultured alone or with pre-plated B78 or MOC2 (2×10^4, 24 hours before) in the 24-well plate with RPMI-1640 (Corning), 1% penicillin/streptomycin (Life Technologies), and 10% FBS (Life Technologies).

After 24 hours, the cells were collected and stained for flow cytometry as described above.

Tumor-secretome preparation and IFN-β-ELISA

To obtain tumor secretomes, tumor cells (5×10^5) were incubated in a 6-well plate for 24 hours. Then, the cells were radiated (0 or 8 Gy for MOC2, and 0 or 12 Gy for B78) 1 hour after AZD0156 (50 nM) stimulation. After 3 or 4 days, the culture media were collected and centrifuged at 5000 rpm for 5 min at 4°C. Then, the supernatants were re-collected and IFN-β-ELISA (BioLegend) was performed following the manufacturer's instruction.

Quantitative messenger RNA analysis

Tumors from mice were dissected and placed in tubes containing 2.8 mm ceramic beads (Fisherbrand) with 1 mL of TRIzol reagent (Invitrogen). Then the tumors were homogenized using a Bead Ruptor Elite (OMNI) for 60 s. The cells treated in vitro were collected using 1 mL of TRIzol reagent (Invitrogen). Total RNA was extracted using the RNeasy Mini Kit (QIAGEN) according to the manufacturer's instructions. Isolated RNA was subjected to complementary DNA synthesis using the QuantiTect Reverse Transcription Kit (QIAGEN) according to the manufacturer's instruction. Quantitative PCR (qPCR) was performed using the CFX96 Real-Time System (Bio-Rad) with PowerUp SYBR Green master mix (Applied Biosystems). Relative messenger RNA (mRNA) expression of target genes was determined according to the 2−ΔΔCT method using *Hprt* as a reference gene.[31] Heatmap was generated by GraphPad Prism software (V.9.5.1) by first sample (1' of STING$^{+/+}$) normalization. The following primer sequences (table 1) were used to detect mRNA expression as previously described.[10 30]

Table 1	Primer sequences list	
Murine	**Primer sequences 5' –3'**	
Genes	**Forward**	**Reward**
Ifnβ (NM_010510.1)	CCCTATGGAGATGACGGAGA	CTGTCTGCTGGTGGAGTTCA
Ccl5 (NM_013653.3)	GAAGGAACCGCCAAGTGTGT	CCTAGCTCATCTCCAAATAGTTGAT
Cxcl9 (NM_008599.4)	CGGACTCGGCAAATGTGAAG	CGACTTTGGGGTGTTTTGGG
Cxcl10 (NM_021274.2)	CTGCCGTCATTTTCTGCCTC	TTCAAGCTTCCCTATGGCCC
Cxcl12 (NM_001012477.2)	CCCTTCAGATTGTTGCACGG	TCTCTGCGCCCCTTGTTTAA
Cxcl16 (NM_023158.7)	TCCTTTTCTTGTTGGCGCTG	TTGGACTGCAACTGGAACCT
Ccl20 (NM_016960.2)	CGACTGTTGCCTCTCGTACA	AGCTTCATCGGCCATCTGTC
Oas2 (NM_001347448.1)	TAAGAGGCTGCTCCGATGGT	GACGTCAAGGTATGCATCTTGGT
Hprt (NM_013556.2)	AGCCTAAGATGAGCGCAAGT	GGCCACAGGACTAGAACACC
Human	**Primer sequences 5' –3'**	
Genes	**Forward**	**Reward**
IFN-β (NM_002176.4)	AAGGCCAAGGAGTACAGT	ATCTTCAGTTTCGGAGGTAA
HPRT (NM_000194.3)	TATGGCGACCCGCAGCCCT	CATCTCGAGCAAGACGTTCAG

STING CRISPR/Cas9 gene editing with RNP complex

crRNA and sNLS-spCas9-sNLS were obtained from IDT. To generate genomic *Sting* (*Tmem173*) KO, the RNP complex containing crRNA and tracrRNA for murine *Sting* was electroporated into 2×10^5 MOC2 or B78 cells using 4D Nucleofector with P3 primary Cell 4D-Nucleofector X kit. After electroporation, the cells were incubated for 48 hours, and a single clone was replated into a 48-well plate. After cell expansion, genomic DNA was extracted using the PureLink Genomic DNA Mini Kit (Invitrogen). The genomic DNA was subjected to Sanger sequencing at the University of Wisconsin Biotechnology Center DNA Sequencing Facility, and the results were analyzed by SnapGene (http://www.snapgene.com) software.

CD8+ T-cell migration assay

Collected tumor-secretomes (300 µL) as described above were placed in the lower chamber of a 24-well transwell plate (CoStar). Freshly sorted CD8+T cells from naïve mouse spleen were prepared in 100 µL of RPMI (Corning) containing 0.5% FBS (Life Technologies) and transferred into the upper chamber (5 µm-pore size). The plates were incubated for 4 hours at 37°C. The number of cells that migrated to the lower chamber were determined using the Countess (Invitrogen) automated cell counter.

Statistical methods

Statistical analysis was done in R V.4.1.2. To analyze the relationships between treatment combinations and longitudinal tumor volumes, linear mixed models were used for each experiment considered and implemented via R packages "lme4" (V.1.1–28) and "lmerTest" (V.3.1–3).[32 33] Each fit log-transformed tumor volume as the response in order to satisfy model assumptions. Mouse ID was fit as a random intercept to account for correlated observations, while the treatment groups, time in days, all two-way interactions, and the three-way interaction comprised the fixed effects. Tukey's honestly significant difference (HSD) method was used to make post hoc pairwise comparisons of the three-way interaction. The R package "survival" (V.3.2–13) was used to analyze time to death data. Survival curves were generated using the Kaplan-Meier method. The log-rank test was used to make pairwise comparisons between curves, and resulting p values were adjusted for multiple comparisons using Benjamini-Hochberg's method. All statistical tests were two-sided, and 5% ($p<0.05$) was set as the level of significance. Observed group differences from qPCR, flow cytometry, ELISA, and proliferation assays were analyzed using analysis of variance, and Tukey's method was used to adjust for p values in post hoc pairwise comparisons. Student's t-test was used for two-sample comparisons.

RESULTS

ATM inhibitor enhances response to tumor-directed radiation in syngeneic tumor models

Tumors that are poorly responsive to immune checkpoint inhibition are often poorly immunogenic, exhibiting few tumor-infiltrating immune cells in the tumor microenvironment and/or limited tumor cell susceptibility to immune recognition and destruction. RT can enhance tumor immune infiltration and tumor cell susceptibility to immune response, in part by activation of an IFN-I response.[34] ATM inhibition is known to sensitize cells to RT, but it is unknown what effect this may have on the immune susceptibility of tumor cells. We first determined whether ATM inhibition could elicit antitumor response when combined with RT on tumor-bearing mice. C57BL/6 mice bearing poorly immunogenic syngeneic B78 melanoma flank tumors were treated with oral administration of AZD0156 and/or 12 Gy of tumor-directed RT (figure 1A). Mice receiving both RT and AZD0156 exhibited a significant reduction in tumor growth compared with mice receiving single treatments or sham/vehicle control treatment (figure 1B,C). This resulted in an increase in survival, consistent with a cooperative antitumor response elicited by RT and AZD0156 treatment in B78 melanoma (figure 1D).

We tested these observations in the poorly immunogenic MOC2 murine HNSCC tumor model (figure 1E).[26] In C57BL/6 mice bearing syngeneic MOC2 flank tumors, the combination of tumor-directed RT (8 Gy) with AZD0156 oral administration showed improved antitumor response compared with single treatments or control groups (figure 1F,G). Similar to the B78 model, this resulted in a significant increase in the survival of MOC2 tumor-bearing mice (figure 1H). The doses of 12 Gy and 8 Gy in the B78 and MOC2 tumor models, respectively, were chosen based on our prior studies in which we had demonstrated the capacity of these doses to elicit an in situ vaccine response in these models.[11 35]

RT and ATM inhibition elicit CD8+ T cell-dependent antitumor response

To determine whether ATM inhibition could enhance the immunogenic effects of RT, we investigated immune cell infiltration in B78 tumor-bearing mice on day 12 following tumor RT and AZD0156 administration. We observed that RT+AZD0156 significantly decreased tumor weight compared with single treatment or vehicle/sham treatment control groups (figure 2A). Immune cell infiltration of tumors was evaluated using flow cytometry (online supplemental figure 1A), which showed that RT+AZD0156 significantly increased the proportion of CD45+tumor-infiltrating cells composed of CD4+, CD8+, and natural killer (NK)1.1+ cells compared with single or control treatment groups (figure 2B). We conducted immune cell depletion in mice bearing syngeneic B78 tumors to test the necessity of specific immune lineages for RT+AZD0156-induced antitumor response (figure 2C). Depletion efficacy was confirmed by peripheral blood collection on day 7 (figure 2D). CD8+, CD4+, or NK cell-depleted mice receiving RT+AZD0156 exhibited significantly
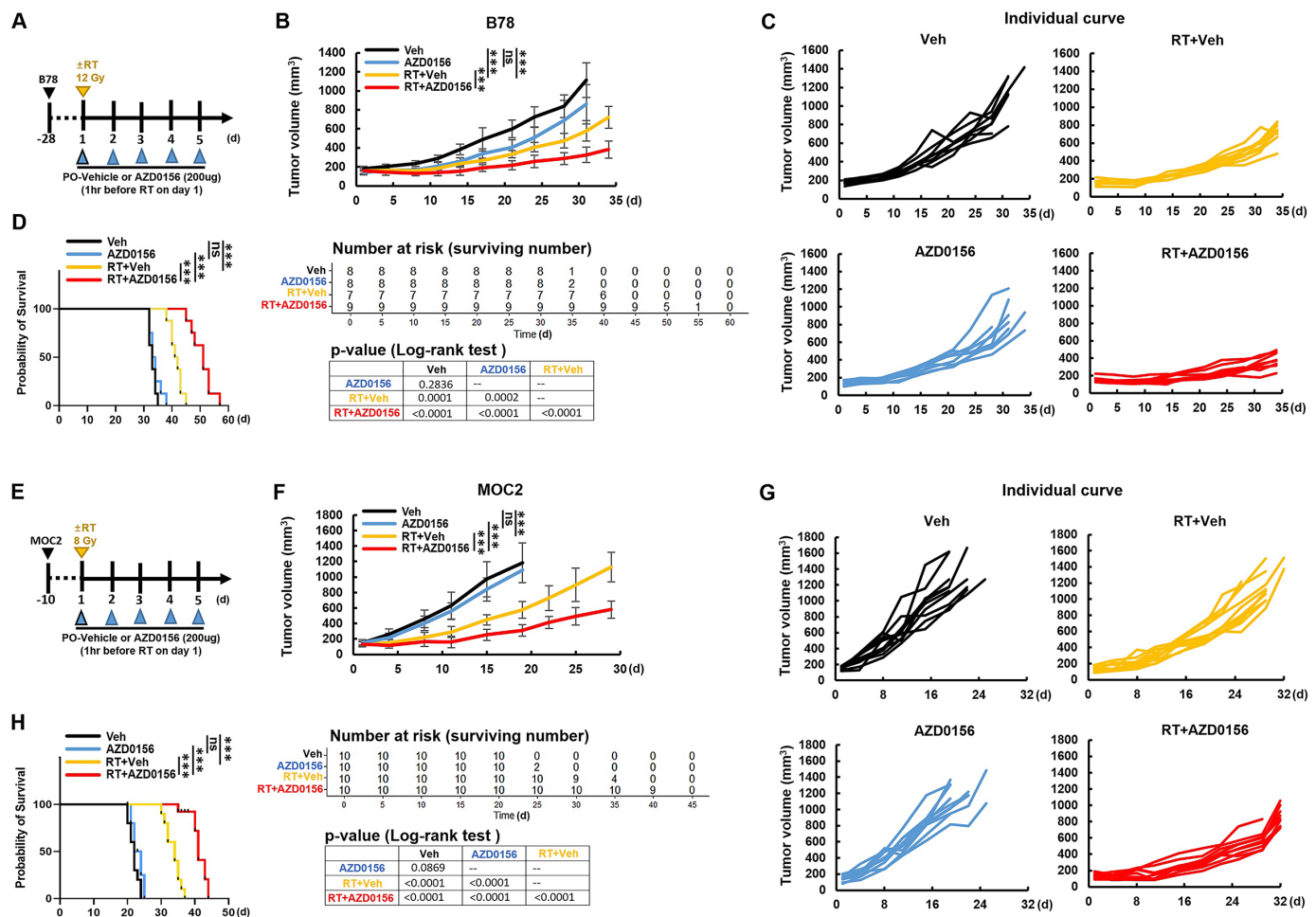
Figure 1 Enhanced tumor response with the combination of tumor-directed RT and systemic administration of AZD0156 in syngeneic murine models of melanoma and head and neck cell carcinoma. (A–D) C57BL/6 mice were engrafted subcutaneously with 2×10^6 B78 cells in the right flank. When the mean tumor volume reached 150–200 mm³, the mice were randomized and treated with local tumor RT (0 or 12 Gy) 1 hour after oral administration of AZD0156 (200 µg) or vehicle control (oil). The mice were further treated with AZD0156 or oil on the indicated day. (n=7–9/group) (A) Treatment regimen, (B) mean tumor volume curves, (C) individual tumor volume curves, and (D) mouse survival data are shown. (E–H) C57BL/6 mice were engrafted with 2×10^6 MOC2 cells in the right flank. When the mean tumor volume reached 150–200 mm³, mice were randomized and treated with local tumor RT (0 or 8 Gy) 1 hour after oral administration of AZD0156 (200 µg) or vehicle control. The mice were further treated with AZD0156 or oil on the indicated day. (n=10/group) (E) Treatment regimen, (F) mean tumor volume curves, (G) individual tumor volume curves, and (H) mouse survival data are shown. Significance was determined by linear mixed-effects analysis with Tukey's multiple comparisons (B, F) and log-rank testing (D and H). Veh, vehicle control. ns, not significant; **p≤0.01; ***p≤0.001. RT, radiation therapy.

reduced tumor response compared with non-depleted mice (figure 2E). Consistently, immune cell depletions reduced survival following RT+AZD0156, demonstrating that immune infiltration is essential to elicit an antitumor response to this treatment combination on B78 tumor-bearing mice (figure 2F).

We next evaluated these observations in MOC2 tumor-bearing mice. We confirmed that RT+AZD0156 effectively decreased tumor weight compared with single treatment or vehicle/sham treatment control groups (figure 2G). We found that RT+AZD0156 significantly increased the proportion of CD45+tumor infiltrating cells composed of CD8+T cells compared with single or control treatment groups, while the proportion of tumor infiltrating CD45+cells that were CD4+T cells, NK cells, and

regulatory T cells were not significantly changed with this treatment combination (figure 2H and online supplemental figure 1B). We conducted CD8+T cell depletion in mice bearing syngeneic MOC2 tumors to test the necessity of CD8+T cells to RT+AZD0156-induced antitumor response (figure 2I). Depletion efficacy was confirmed by peripheral blood collection on day 15 (figure 2J). Mice receiving RT+AZD0156 and depleted of CD8+T cells exhibited significantly reduced tumor response compared with those receiving RT+AZD0156 without CD8+T cell depletion (figure 2K). Consistently, CD8+T cell depletion reduced survival following RT+AZD0156, demonstrating that CD8+T cells are necessary for the antitumor response to this treatment combination on MOC2 tumor-bearing mice (figure 2L).
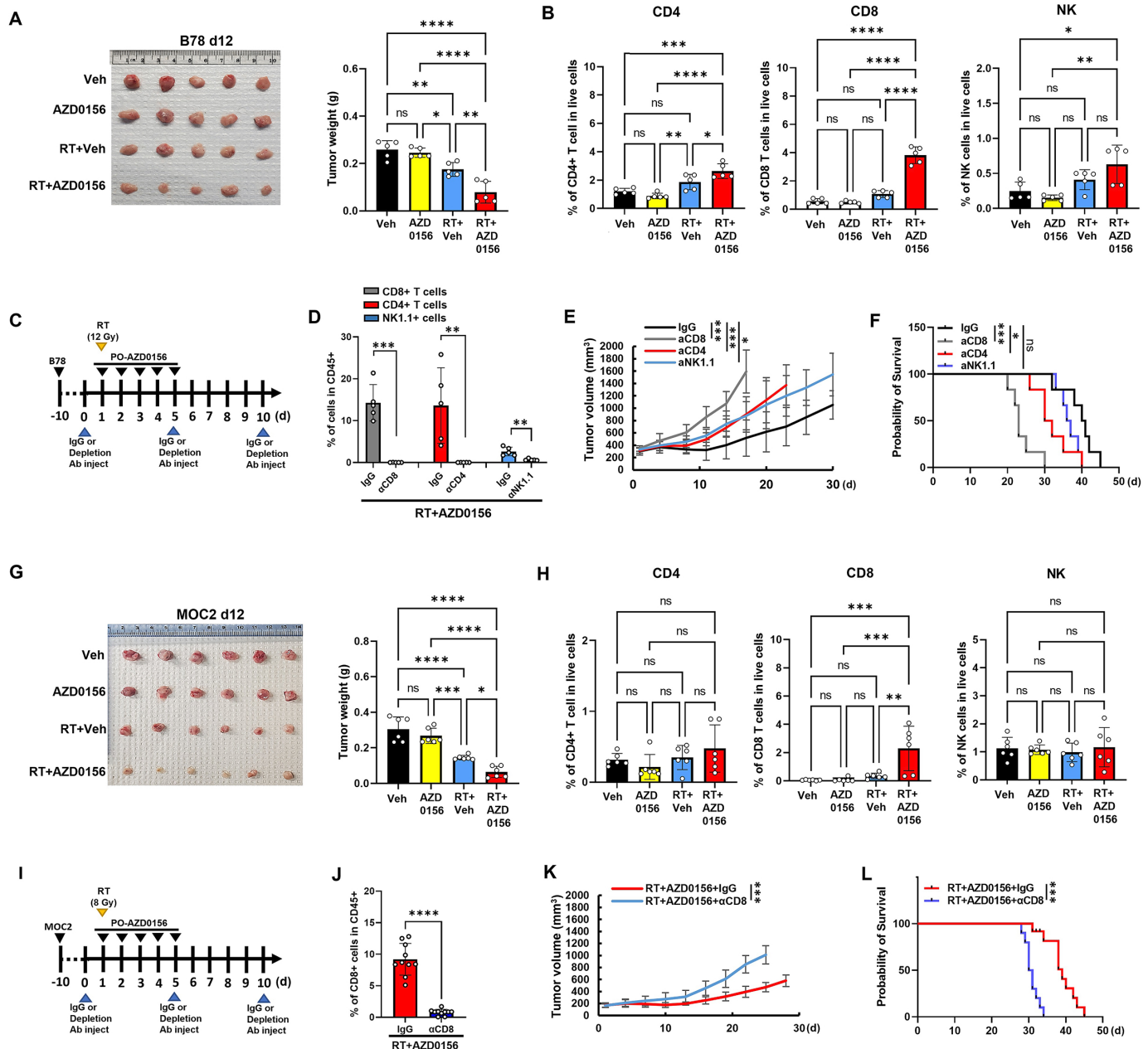
Figure 2 Combined RT and AZD0156 induces CD8+T cell-mediated antitumor response. (A–B) C57BL/6 mice were engrafted with a B78 tumor in the right flank and treated as in figure 1. (A) Tumors were dissected and weighed on day 12 after treatment initiation (B) Flow cytometry was used to quantify the proportion of lymphocyte lineages among CD45+tumor infiltrating immune cells (live+CD45+CD3+CD4+/CD8+ or live+CD45+CD3−NK1.1+). (C–G) C57BL/6 mice bearing a B78 tumor were treated as in figure 1A. During treatment, an anti-CD4− (clone GK1.5, 300 µg), CD8a− (clone 2.45, 300 µg), or NK1.1 (clone PK136, 50 µg) depleting antibody or non-specific control IgG antibody (300 µg) was injected intraperitoneally on day 0, 5, and 10. (C) Treatment regimen is depicted. (D) Depletion efficiency was confirmed using flow cytometry on blood of mice at treatment day 7. (E) Mean tumor volume curves and (F) mouse survival data are shown. (n=5/group) (G–H) C57BL/6 mice were engrafted with an MOC2 tumor in the right flank and treated as in figure 1. (G) Tumors were dissected and weighed on day 12 after treatment initiation. (H) Flow cytometry was used to quantify the proportion of lymphocyte lineages among CD45+tumor infiltrating immune cells (live+CD45+CD3+CD4+/CD8+ or live+CD45+CD3−NK1.1+). (I–L) C57BL/6 mice bearing a MOC2 tumor were treated as in figure 1A. During treatment, an anti-CD8a depleting antibody (clone 2.45, 300 µg) or non-specific control IgG antibody (300 µg) was injected intraperitoneally on day 0, 5, and 10. (I) Treatment regimen is depicted. (J) CD8+T cell depletion efficiency was confirmed using flow cytometry on blood of mice at treatment day 7. (K) Mean tumor volume curves and (L) mouse survival data are shown. (n=10/group) Significance was determined by one-way analysis of variance with post hoc Tukey's (A) B) G) and (H) two-tailed student's t-test (D and J) linear mixed-effects analysis with Tukey's multiple comparisons (E and K) and log-rank testing (F and G). Veh, vehicle control. ns, not significant; *p≤0.05; **p≤0.01; ***p≤0.001. NK, natural killer; RT, radiation therapy.

ATM inhibition increases radiosensitivity and type I interferon expression following RT

Given that AZD0156 administration alone showed no impact on tumor growth in B78 and MOC2 tumor-bearing mice, we determined a dose of AZD0156 that did not affect tumor cell proliferation in vitro. We cultured B78, MOC2, and the human HNSCC cell line SCC6 in the presence of increasing AZD0156 or vehicle control treatments. We observed that low-dose AZD0156 (1–100 nM) did not affect tumor cell viability/proliferation for MOC2, B78, or SCC6, but high-dose (1000 nM and/or 2000 nM) significantly decreased the cell viability/proliferation in these tumor lines (figure 3A–C). Because we observed that combined AZD0156 and local tumor radiation synergistically increased antitumor response compared with AZD0156 alone in vivo, we tested the potential impact of the non-toxic, low-dose AZD0156 (50 nM) on the intrinsic radiosensitivity of tumor cells in vitro. While AZD0156 (50 nM) alone did not affect clonogenicity of MOC2, B78, or SCC6 cells, combined AZD0156 and RT increased the radiosensitivity of tumor cells and inhibited clonogenic potential (figure 3D–F).

To further understand the interaction of RT and AZD0156, we tested whether AZD0156 could directly increase immune susceptibility of tumor cells by activating an IFN-I response. For this, we stimulated MOC2 cells with AZD0156 and quantified the expression of *Ifnβ* mRNA using qPCR. We observed that AZD0156 alone did not stimulate *IFN-β* expression after 24-hour culture (figure 3G). It is known that RT at 8 Gy can activate an IFN-I response in tumor cells, including MOC2 cells.[11] Given the capacity of low-dose AZD0156 to radiosensitize MOC2 cells, we evaluated whether this agent would also augment the activation of *Ifnβ* by RT. Intriguingly, low-dose AZD0156 (50 nM) increased *Ifnβ* expression in MOC2 cells following 8 Gy RT.

Given the known role of RT in activating transcription of *Ifnβ* via cGAS/STING pathway mediated detection of cytosolic dsDNA, we investigated whether RT and AZD0156 can increase cytosolic dsDNA in MOC2 cells. We observed that AZD0156 synergistically enhanced the accumulation of cytoplasmic dsDNA on tumor radiation (figure 3H). In addition, we observed that RT+AZD0156 promoted IFN-β secretion in MOC2 cells (figure 3I). Our in vitro data showed that AZD0156 doses 1–100 nM have no cytotoxicity on the tumor cells and induce no *Ifnβ* mRNA expression change compared with vehicle control. Intriguingly, the non-cytotoxic AZD0156 50 nM dose showed a cooperative increase in *Ifnβ* mRNA when combined with in vitro RT. As our in vivo data showed no tumor growth inhibition following 200 µg of AZD0156 administration alone but suppressed tumor growth by a combination of RT and AZD0156, we tested whether in vivo treatment with combined RT and AZD0156 could elicit a cooperative increase in IFN-β mRNA in MOC2 tumors. When RT and AZD0156 treatment was given to MOC2 tumor-bearing mice, we observed that AZD0156 increased *Ifnβ* expression in tumors compared with vehicle, AZD0156, or RT

treatment alone. We hypothesized that increased cytosolic dsDNA results from AZD0156 inhibition of DNA damage repair. Consistent with this, we observed that in vivo RT of MOC2 tumors elicits increased γH2AX phosphorylation, a marker of initiation of DNA damage repair, but AZD0156 together with RT suppressed γH2AX induction (figure 3K). These results demonstrate that following RT, AZD0156 suppresses DNA damage repair, increases cytosolic dsDNA, and increases expression of *Ifnβ*.

To evaluate functional effects of tumor cell treatment with RT+AZD0156 on T cells, we tested naïve CD8+T cell viability after co-culture with MOC2 cells that had been treated with RT+AZD0156 (online supplemental figure 2A).[36] RT+AZD0156 treatment of MOC2 cells significantly increased the number of live CD8+T cells following co-culture, compared with MOC2 cells treated with vehicle, AZD0156 alone, or RT+vehicle (online supplemental figure 2B). Compared with vehicle, AZD0156, and/or RT+vehicle, RT+AZD0156-treated MOC2 cells promoted CD69+ and IFN-γ+ cells in naïve CD8+T cells (online supplemental figure 2C). These observations suggest that the effects of RT+AZD0156 in modifying the immunogenicity (eg, *Ifnβ* expression) of MOC2 cells is sufficient to promote favorable phenotypic changes in nearby CD8+T cells. In an initial assessment of the generalizability and duration of these immunogenic effects on tumor cells, we confirmed that low-dose AZD0156 (50 nM) similarly enhanced RT-stimulated *Ifnβ* expression in MOC2, B78, and human SCC6 cells at 72 hours after RT (figure 3L–N). These results suggested a potential immunologic benefit of combining AZD0156 and RT to elicit IFN-I induction in an irradiated tumor.

AZD0156+RT influences tumor infiltrating CD8+ T cells

Previous reports demonstrated that IFN-I activates granzyme B (GZMB) expression in cytotoxic lymphocytes (CTLs), and IFNAR1-KO reduces GZMB transcription in CTLs.[37] In addition, IFN-I stimulates early activation marker CD69 expression in lymphocytes via IFNAR1.[38] Given that the tumor-derived IFN-I could elicit an immune response, we first evaluated infiltrated CD8+T cell responses from MOC2 tumor-bearing mice on day 12 after RT and/or AZD0156 treatment, as indicated in figure 2A. Combined RT and ATM0156 treatment significantly upregulated CD69 and the cytotoxic enzyme GZMB in CD8+T cells compared with other treatment regimens (figure 4A).

We next investigated whether the effect of RT+AZD0156 in enhancing CD8+T cell tumor infiltration was dependent on an IFN-I response. For this, MOC2 tumor cells were engrafted on the wild type (WT) or IFNAR1-deficient (IFNAR1-KO) mice, respectively. When RT+AZD0156 treatment was given to MOC2 tumors in WT mice, we observed that this treatment resulted in an increase in the proportion of CD45+cells composed of CD8+T cells in tumor-infiltrating immune cells on day 12 after RT (figure 4B). In contrast, mice lacking IFNAR1 did not show this response and showed no change in the fraction
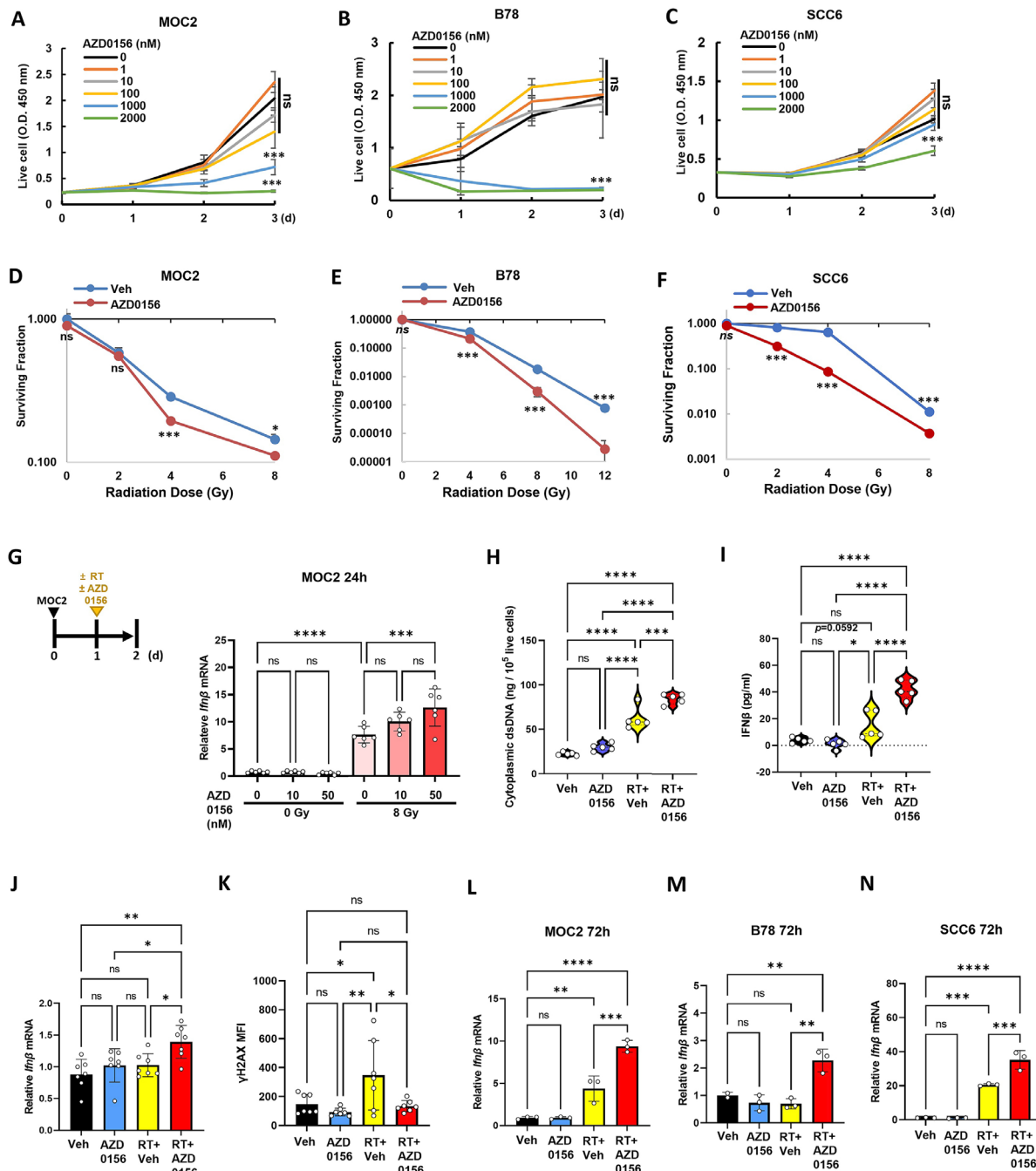
Figure 3 AZD0156 increases tumor cell radiosensitivity and increases the type I interferon response following RT. (A–C) Tumor cells were cultured in the presence of indicated concentrations of AZD0156 or vehicle control (DMSO). At the indicated time point (day 0, 1, 2, and 3), (A) MOC2, (B) B78, or (C) SCC6 viable cells were quantified. (n=3/group) (D) Pre-plated tumor cells were radiated with indicated doses (0, 2, 4, 8, or 12 Gy), then the cells were replated in the presence of AZD0156 (50 nM) or DMSO for 7–10 days. The clonogenic colonies were quantified and are displayed as a percent of total replated cells for (D) MOC2, (E) B78, or (F) SCC6. (n=3/group) (G) MOC2 cells were radiated with 0 or 8 Gy in the presence of indicated concentrations of AZD0156 (0, 10, or 50 nM). After 24 hours, the cells were collected and analyzed for relative *Ifnβ* mRNA expression using qPCR. (n=5/group). (H and I) MOC2 cells were radiated with 0 or 8 Gy 1 hour after treatment with DMSO vehicle or AZD0156 (50 nM). After 24 hours, the cells and supernatants were collected and quantified for (H) cytoplasmic dsRNA in the cells and (I) IFN-β production in the supernatants. (J and K) MOC2-bearing mice were treated with tumor-directed RT (0 or 8 Gy) 1 hour after oral administration of AZD0156 (200 μg) or vehicle control. After 24 hours, tumors were dissected and analyzed for (J) *Ifnβ* mRNA expression in tumor and (K) γH2AX MFI in Live CD45− cells. (L–N) The indicated tumor cells were irradiated (0 or 8 Gy for MOC2/SCC6, 0 or 12 Gy for B78) in the presence of AZD0156 (50 nM) or DMSO vehicle control. After 3 days, the cells were collected, and relative *Ifnβ* mRNA expression was quantified by qPCR. (n=3/group) Significance was determined by two-tailed student's t-test (A–F), and one-way analysis of variance with post hoc Tukey's (G–N). Veh, vehicle control. ns, not significant; *p≤0.05; **p≤0.01; ***p≤0.001, ****p≤0.0001. dsDNA, double stranded DNA; IFN, interferon; mRNA, messenger RNA; qPCR, quantitative PCR; RT, radiation therapy; DMSO, dimethyl sulfoxide; MFI, median fluorescence intensity.
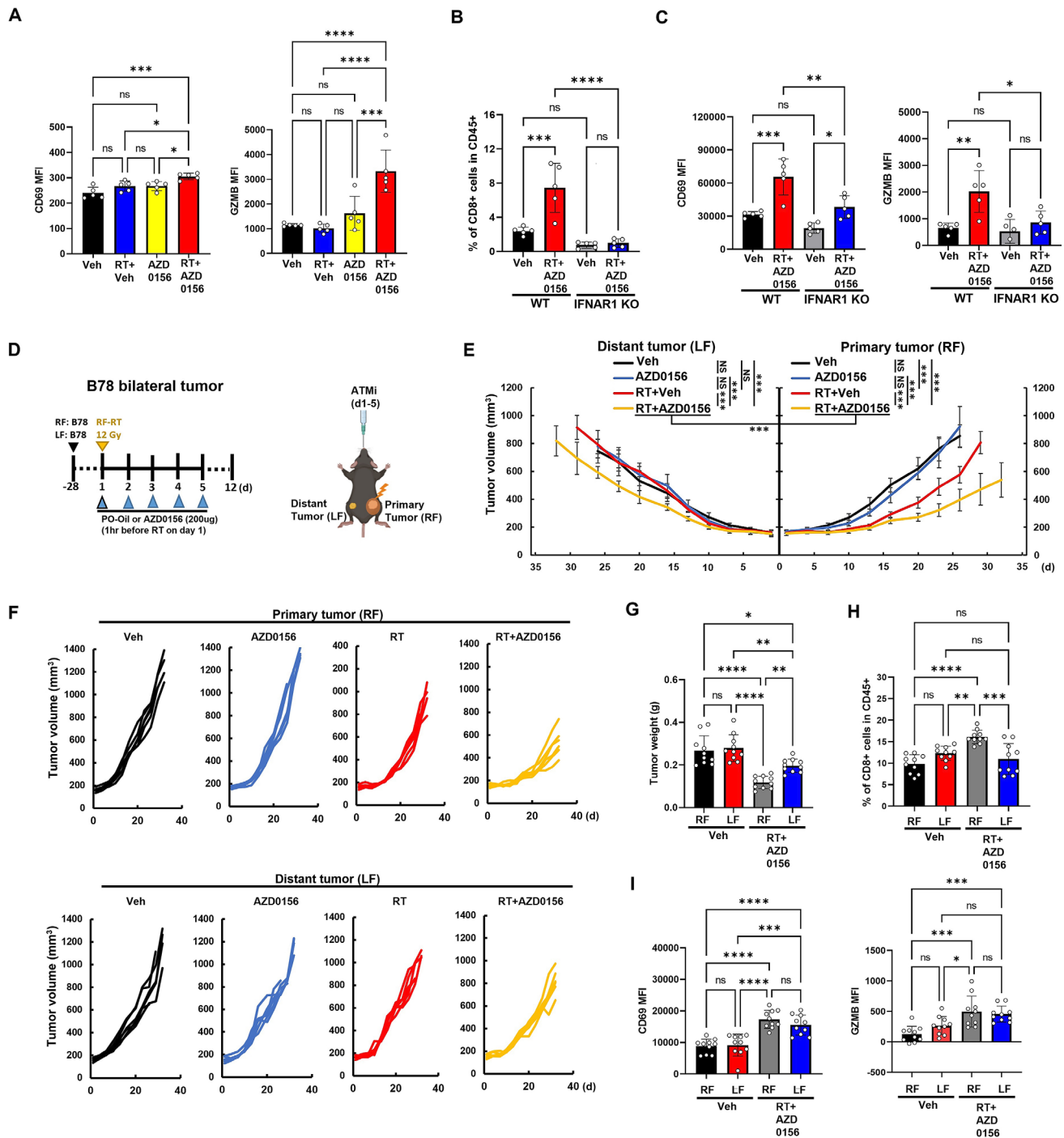
Figure 4 CD8+T cell infiltration requires type I interferon signaling following AZD0156 with tumor radiation. (A) C57BL/6 mice were engrafted subcutaneously with MOC2 tumors in the right flank and treated as per figure 1A. Tumors were collected on day 12 after treatment initiation and flow cytometry was used to evaluate the expression of CD69 and GZMB on CD8+T cells. (n=5/group) (B) and (C) WT or type 1 interferon receptor 1 knock-out (IFNAR1-KO) C57BL/6 mice were engrafted subcutaneously with MOC2 in the right flank and treated as in figure 1A. Tumors were collected on day 12 after treatment initiation and flow cytometry was used to quantify (B) CD8+T cell infiltration and (C) the expression of CD69 and GZMB on these. (n=5/group) (D–H) C57BL/6 mice were engrafted subcutaneously with B78 in the right flank (RF) and the left flank (LF). When the bilateral tumor-bearing mice reached a mean tumor volume of 150–200 mm^3, the mice were randomized and treated on the RF-tumor with RT (0 or 12 Gy) 1 hour after control vehicle or AZD0156 (200 µg) administration. The mice were further injected with AZD0156 or control vehicle on the indicated day. (D) Treatment regimen is depicted and (E) mean and (F) individual tumor volume curves are shown. (n=7/group) (G) RF and LF tumors were dissected and weighed on day 12 after treatment initiation. Flow cytometry was used to quantify (H) tumor-infiltrating CD8+T cells and (I) the expression of CD69 and GZMB on these. (n=10/group) Significance was determined by one-way analysis of variance with post hoc Tukey's (A–C, F–H) and linear mixed-effects analysis with Tukey's multiple comparisons (E). Veh, vehicle. ns, not significant; *p≤0.05, **p≤0.01; ***p≤0.001, ****p≤0.0001. ATMi, ataxia-telangiectasia mutated inhibitor; GZMB, granzyme B; RT, radiation therapy; WT, wild type; MFI, median fluorescence intensity.

of CD8+T cells among CD45+cells in tumor-infiltrating immune cell populations when compared with vehicle control-treated mice. We further observed that IFNAR1 was necessary for the effect of RT+AZD0156 in increasing the expression of CD69 and GZMB in tumor-infiltrating CD8+T cells (figure 4C).

Given the observation of CD8+T cell infiltration and activation following RT+AZD0156, we evaluated whether this treatment combination would elicit an antitumor response at a non-radiated tumor site in mice bearing multiple tumors. To model metastatic disease, we engrafted B78 tumors on the "primary" right flank and the "distant" left flank of mice. We then treated mice with a combination of AZD0156 and 12 Gy RT that targeted the primary tumor while the distant tumor was shielded with lead (figure 4D). In this poorly immunogenic bilateral tumor model, we observed that primary tumor RT+systemic AZD0156 administration still yielded a small but significantly improved antitumor response over RT or AZD0156 monotherapy in the non-radiated distant tumor; however, this non-radiated distant tumor response was significantly reduced compared with the primary tumor (figure 4E,F). Likewise, monotherapy radiation or AZD0156 yielded no significant difference in distant tumor growth compared with vehicle (figure 4E,F). These observations indicate that in this tumor model RT or AZD0156 monotherapy has no antitumor response on non-radiated tumor growth while combined RT+AZD0156 has a significantly reduced effect on non-radiated distant tumor growth.

Consistent with this treatment response data, primary tumor RT+systemic AZD0156 increased CD8+T cell infiltration in the primary B78 tumor but did not change infiltration of the distant tumor compared with mice receiving sham/vehicle control treatments (figure 4G). In the primary tumor, RT+AZD0156 significantly increased GZMB expression among tumor-infiltrating CD8+T cells compared with sham/vehicle control treated mice, whereas tumor infiltrating CD8+T cells in the distant tumor showed no significant change in GZMB expression compared with control mice (figure 4H). Interestingly, we did observe upregulation of the early T-cell activation marker, CD69, on the surface of tumor-infiltrating CD8+T cells at both the primary and distant tumor sites following primary tumor RT+AZD0156, when compared with sham/vehicle-treated control mice. These observations suggest that primary tumor RT+systemic AZD0156 can initiate CD8+T cell effector activation, but this is insufficient to achieve antitumor response in the non-radiated distant tumor.

Increased MHC-I and PD-L1 expression following RT+AZD0156 is STING-dependent

It has been reported that ATM inhibition promotes STING activation in the murine 4T1 breast cancer and B16 melanoma models.[23] Given our observation that AZD0156 augments the IFN-I response in tumor cells following RT, we sought to determine whether STING was necessary for the antitumor immune response elicited by RT+AZD0156.

For this purpose, we generated a homozygous STING deletion mutant of B78 melanoma (figure 5A,B) and a heterozygous STING deletion mutant of MOC2 using the CRISPR KO system (online supplemental figure 3A). We confirmed that STING protein was non-detectible in the B78-STING$^{-/-}$ cells (figure 5C) or weakly detectible in the MOC2-STING$^{+/-}$ (online supplemental figure 3B). In addition, RT-induced phosphorylation of γH2AX, a DNA damage repair marker, was reduced by ATM inhibition in both WT and STING deficient B78 or MOC2 cells, suggesting that AZD0156 suppressed the RT-induced DNA repair response. We observed that B78-STING$^{+/+}$ cells secreted IFN-β after RT or RT+AZD0156; however, this treatment-response did not occur in B78-STING$^{-/-}$ cells (figure 5D) or MOC2-STING$^{+/-}$ cells (online supplemental figure 3C).

Previous reports suggest that IFN-β stimulation increases PD-L1 expression.[39 40] In addition, IFN-β can increase MHC-I expression on tumor cells.[41] RT has been shown to upregulate both PD-L1 and MHC-I on tumor cells[42 43] and such effects may result from STING-dependent[44] and STING-independent pathways.[45] Given that RT+AZD0156 can stimulate STING-dependent IFN-β secretion, we evaluated the effects of RT+AZD0156 on tumor cell PD-L1 and MHC-I expression. We observed that this treatment combination increased PD-L1 and MHC-I expression in WT tumor cells; however, STING-deficiency antagonized this effect in B78 (figure 5E) and MOC2 cells (online supplemental figure 3E). We next evaluated mRNA levels of a panel of IFN-inducible chemokines that are well-known factors that elicit T-cell chemotaxis.[46–49] On RT+AZD0156 stimulation, STING-deficient tumors (B78-STING$^{-/-}$ or MOC2-STING$^{+/-}$) showed a reduction of CCL5, CXCL9, and CXCL10 chemokine mRNA compared with WT cells (figure 5F and online supplemental figure 3F). Consistently, tumor-secretomes collected from STING-deficient tumor cells showed a reduction of CD8+T cell migratory effects compared with the WT tumor-secretomes (figure 5G and online supplemental figure 3G).

We evaluated the effects of STING deficiency on the response to RT+AZD0156 in vivo using the B78-STING$^{-/-}$ and B78-STING$^{+/+}$ tumor models. We observed that in the absence of any treatment B78-STING$^{-/-}$ tumors exhibited similar growth rates when compared with B78-STING$^{+/+}$ tumors (figure 5H). However, following treatment with RT+AZD0156, B78-STING$^{-/-}$ tumor-bearing mice showed significantly reduced antitumor response compared with B78-STING$^{+/+}$ tumor-bearing mice, and this resulted in significantly reduced survival in B78-STING$^{-/-}$ tumor-bearing mice (figure 5I,J). We observed a significant reduction in B78-STING$^{-/-}$ tumor infiltration by CD8+T cells (figure 5K) and in the expression of CD69 and GZMB in tumor-infiltrating CD8+T cells, as compared with B78-STING$^{+/+}$ tumors (figure 5L). These data suggest that tumor cell expression of STING is essential to the cooperative therapeutic effects of RT and AZD0156 in stimulating antitumor response and adaptive antitumor immunity.
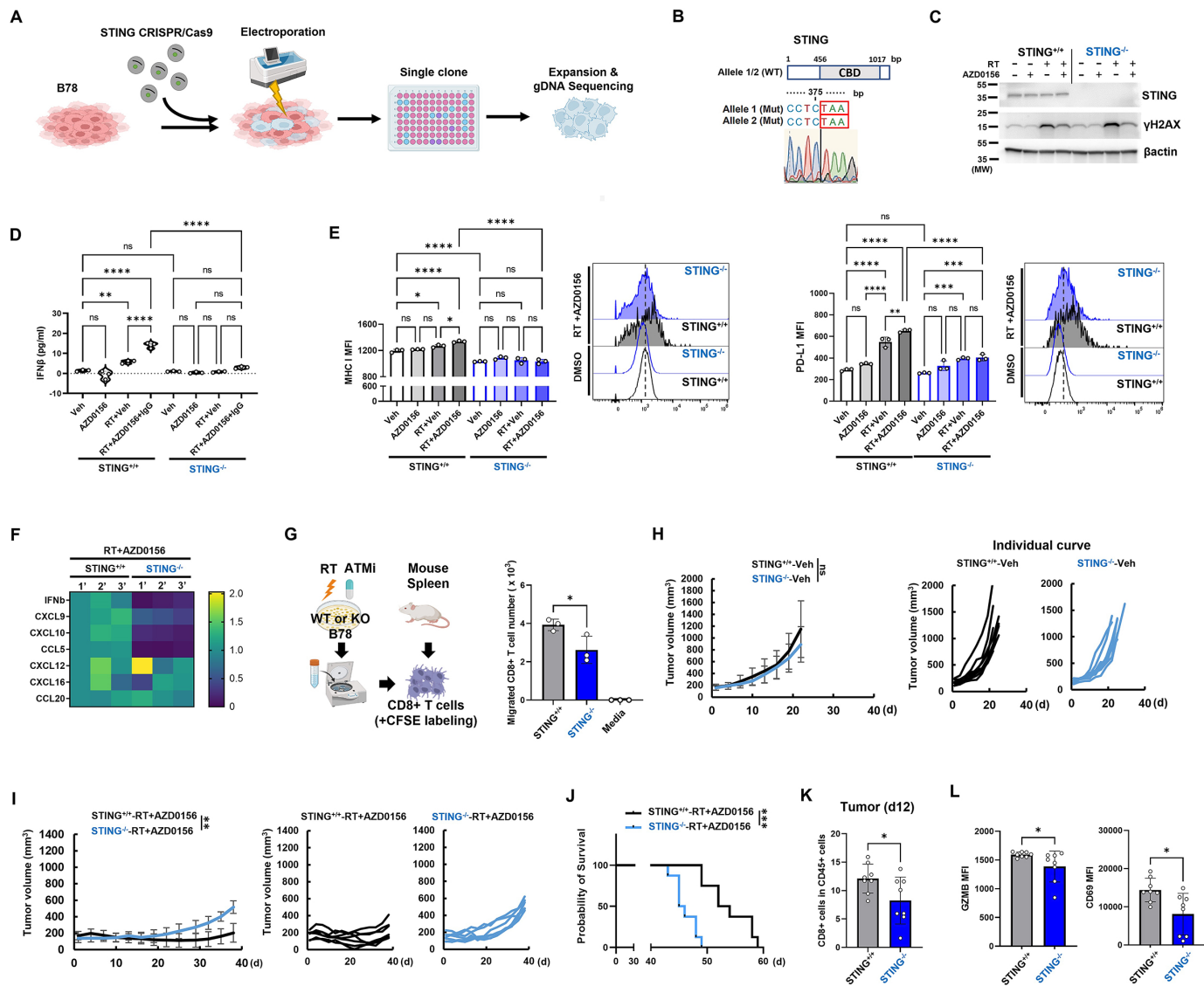
Figure 5 AZD0156 enhances RT-stimulated, STING-dependent, type 1 interferon response in tumor cells. (A–C) B78 cells were transduced to delete genomic *Sting* (*Tmem173*) using electroporation of recombinant Cas9 and guide RNA. The single sorted clone was expanded and sequenced. (A) Scheme of the procedures for the STING CRISPR/Cas9 genomic editing procedure is depicted. (B) STING genomic DNA sequence of WT and STING KO alleles is shown. (C) B78 cells were radiated (0 or 12 Gy) 1 hour after DMSO vehicle or AZD0156 (50 nM) pretreatment. After 0.5 hour of incubation, the cells were lysed, and western blot was performed to determine STING, γH2AX, and β-actin protein levels. (D–G) B78-STING$^{+/+}$ or B78-STING$^{-/-}$ cells were treated with DMSO (Veh), RT (12 Gy), AZD0156 (50 nM) and/or RT+AZD0156. (D) The culture supernatants were collected and analyzed for IFN-β production by ELISA. (E) Cell surface expression of MHC-I and (G) PD-L1 were analyzed by flow cytometry. (F) Relative mRNA expression was analyzed and represented. (G) Tumor-secretome collected from RT+AZD0156-treated B78 cells or media was placed in the lower chamber (300 µL) of a 24-well transwell plate. Sorted CD8+T cells prepared in 100 µL of the media were transferred into the upper chamber (5 µm-pore size). After 4-hour incubation, the number of cells that migrated to the lower chamber was determined. (H–L) C57BL/6 mice were engrafted subcutaneously with B78-STING$^{+/+}$ or B78-STING$^{-/-}$ cells in the right flank and treated as indicated in figure 1A. (H) Tumor growth curves, (I) individual tumor volume curves, and (J) mouse survival data are shown. (n=7/group) (K) and (L) Tumors from another cohort of mice, all treated with RT+AZD0156, were collected on day 12. (J) Tumor-infiltrating CD8+T cells and (K) MFI of GZMB and CD69 in the tumor-infiltrating CD8+T cells were analyzed by flow cytometry. (n=8/group) Significance was determined by two-tailed student's t-test (G) K) and (L) one-way analysis of variance with post hoc Tukey's (D and E) linear mixed-effects analysis with Tukey's multiple comparisons (H) and (I)-left, and log-rank testing (I)-right. Veh, vehicle. ns, not significant; *p≤0.05; **p≤0.01; ***p≤0.001; ****p≤0.0001.ATMi, ataxia-telangiectasia mutated inhibitor; GZMB, granzyme B; IFN, interferon; KO, knockout; MHC, major histocompatibility complex; mRNA, messenger RNA; PD-L1, programmed death-ligand 1; STING, stimulator of interferon genes; RT, radiation therapy; WT, wild type; DMSO, dimethyl sulfoxide; CFSE, carboxyfluorescein succinimidyl ester; MFI, median fluorescence intensity.
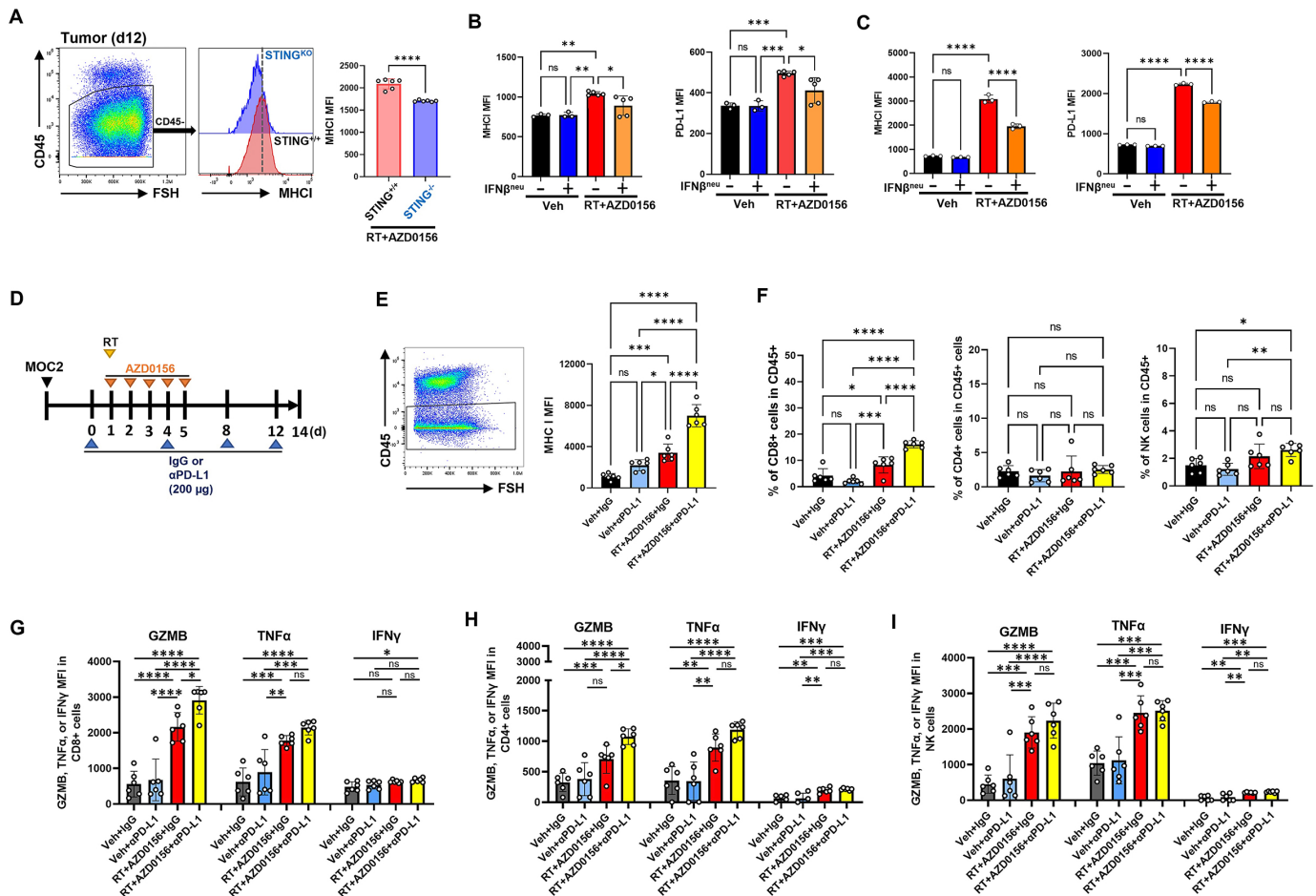
Figure 6 IFN-β response stimulated in tumor cells by RT and AZD0156 increases tumor cell expression of MHC-I and PD-L1 and enhances response to anti-PD-L1 therapy in poorly immunogenic tumor models. (A) Tumors from another cohort of mice from figure 5K were collected on day 12 and MHC-I MFI in the live-CD45 negative cells was analyzed. (B) B78 or (C) MOC2 cells were radiated (0 or 12 Gy for B78, and 0 or 8 Gy for MOC2) 1 hour after control vehicle or AZD0156 (50 nM) pretreatment. Then, control IgG or anti-IFN-β neutralization antibody (clone 1176D, 5 µg/mL) was added. After 3 days, the cells were collected and expression of MHC-I and PD-L1 were analyzed. (D–I) C57BL/6 mice were engrafted subcutaneously with 2×10^6 MOC2 cells in the right flank. When the mean tumor volume reached 150–200 mm^3, the mice were randomized and treated with local tumor RT (0 or 8 Gy) 1 hour after oral administration of AZD0156 (200 µg) or oil. The mice were further treated with AZD0156, oil, intraperitoneal IgG or anti-PD-L1 (clone B7-H1, 200 µg) antibody as indicated. (n=10/group) (D) Treatment regimen is depicted. (E–I) Tumors were collected on day 14 and (E) flow cytometry was used to analyze MHC-I in non-immune cells from the tumors (CD45–negative), (F) tumor-infiltrating lymphocytes, and MFI of cytokines in (G) CD8+T cell, (H) CD4+T cell, and (I) NK cell were analyzed. Significance was determined by two-tailed student's t-test (A) or one-way analysis of variance with post hoc Tukey's (B–I). Veh, vehicle. ns, not significant; *p≤0.05; **p≤0.01; ***p≤0.001; ****p≤0.0001. GZMB, granzyme B; IFN, interferon; MHC, major histocompatibility complex; NK, natural killer; PD-L1, programmed death-ligand 1; STING, stimulator of interferon genes; RT, radiation therapy; TNF, tumor necrosis factor; FSH, forward scatter; MFI, median fluorescence intensity.

Addition of anti-PD-L1 therapy promotes MHC-I expression in tumor and immune activation following RT+AZD0156 therapy

In B78 tumor-bearing mice (figure 5I), we observed that STING deficiency reduced MHC-I expression on CD45– cells (non-immune cells) isolated from tumor (figure 6A). Given that RT+AZD0156 can promote STING-dependent IFN-β, PD-L1, and MHC-I induction in tumors, we sought to determine whether released IFN-β from these tumor cells was responsible for induction of PD-L1 and MHC-I expression. Using an IFN-β neutralizing antibody during RT+AZD0156 treatment, we observed that IFN-β was necessary for the induction of MHC-I and PD-L1 expression following this combined treatment regimen in B78

(figure 6B) and MOC2 cells (figure 6C). This indicated that the induction of IFN-I response by RT+AZD0156 could lead to MHC-I and PD-L1 upregulation on tumor cells by cell autonomous regulation, and we hypothesized that this could contribute to the failure of this treatment regimen to generate an effective systemic antitumor immune response.

Given that tumor-derived IFN-β stimulates PD-L1, an immune exhaustion ligand, we evaluated the effect of anti-PD-L1 antibody therapy when given together with RT+AZD0156 in MOC2 tumor-bearing mice (figure 6D). On day 14, after completion of treatment in MOC2 tumor-bearing mice, we observed that RT+AZD0156+anti-PD-L1

significantly increased tumor MHC-I expression compared with RT+AZD0156 alone or anti-PD-L1 alone (figure 6E). RT+AZD0156+anti-PD-L1 treatment also promoted greater CD8+T cell and NK cell infiltration of the tumor but did not change the levels of infiltration by CD4+T cells (figure 6F). Interestingly, compared with RT+AZD0156 treatment, RT+AZD0156+anti-PD-L1 treatment increased GZMB expression in CD4+ and CD8+ cells but not NK cells (figure 6G–I). We also observed that RT+AZD0156 or RT+AZD0156+anti-PD-L1 increased the expression of the cytotoxic cytokines tumor necrosis factor-α and IFN-γ in CD4+T cells, CD8+T cells, and NK cells (figure 6G–I). These observations suggest that additional anti-PD-L1 therapy elicits activation of tumor infiltrating lymphocytes and MHC-I expression in tumor.

Combining RT+AZD0156 with anti-PD-L1 therapy promotes antitumor immune responses

Given that anti-PD-L1 therapy promoted immune response, we evaluated the antitumor efficacy of anti-PD-L1 therapy following RT and AZD0156 in MOC2 or B78 tumor-bearing mice (figure 7A–G). We observed that RT+AZD0156+anti-PD-L1 significantly suppressed tumor growth with improved survival compared with treatment of RT+AZD0156+IgG or RT+Veh+anti-PD-L1.

To further understand the mechanism by which the combination of RT+AZD0156+anti-PD-L1 suppresses tumor growth, we evaluated the specificity of the antitumor immunity generated by this regimen. We isolated CD8+T cells from the spleen after RT+AZD0156+anti-PD-L1 and cultured them alone or in combination with MOC2 or B78 tumor cells (figure 7I). We observed increased GZMB+ and IFN-γ+ CD8+ T cells following co-culture with MOC2 but not on co-culture with B78 or alone (figure 7J). We further analyzed the CD8+T cell subset by examining CD62L and CD44 expression (figure 7K), which define the roles of T cells as they move from naïve to effector and memory T cells.[50 51] Interestingly, we observed high proportions of the naïve CD62L–CD44+CD8+ T cells and the normally rare CD62L–CD44– CD8+T cells, which are associated with the transition from naïve to effector T cells, and that these proportions were not changed when the T cells were cultured with tumor cells (figure 7L,M). We found that both of these CD8+T cell subsets showed tumor-specific induction of GZMB+cells and of IFN-γ+ cells following MOC2 co-culture compared with CD8+T cells alone or B78 co-culture (figure 7L,M). We investigated the effects of αPD-L1 therapy in the non-radiated tumor following treatment of the primary tumor with RT+AZD0156 (online supplemental figure 4A). We observed that the combination of RT+AZD0156+αPD-L1 therapy promoted antitumor response in the non-radiated tumor compared with RT, RT+AZD0156, or RT+αPD-L1 treatment regimens (online supplemental figure 4B,C). These observations indicate that a combination of local tumor radiation, oral administration of AZD0165, and systemic αPD-L1 antibody therapy promotes systemic antitumor response in non-radiated tumors.

DISCUSSION

We demonstrate that a combination of RT and ATM inhibition elicited enhanced antitumor immunity in murine syngeneic tumor models of poorly immunogenic melanoma and HNSCC. Our results suggest that RT+AZD0156 stimulated enhanced antitumor immunity compared with RT alone. This effect was dependent on tumor cell expression of STING and host immune cell expression of IFNAR1 but was limited by IFN-β-induced PD-L1 expression. Immune checkpoint inhibition with anti-PD-L1 antibody therapy enhanced response to RT+AZD0156, and the antitumor immune response generated by RT+AZD0156, in turn, augmented response to anti-PD-L1 therapy in poorly immunogenic tumor models.

ATM inhibition has been demonstrated to elicit cell cycle arrest and cytotoxicity in tumors[52] and we observed such effects on both tumor and immune cells with higher concentrations of AZD0156 in vitro. However, at lower concentrations of AZD0156 (1–100 nM) in vitro, we observed that ATM inhibition alone resulted in minimal monotherapy response but such concentrations could enhance the activation of an IFN-I response by RT in tumor cells. Similarly, when combined with RT in vivo, we observed that a dose of AZD0156 that did not achieve monotherapy efficacy was sufficient to significantly delay tumor growth, extend mouse survival, and increase tumor infiltration by CD8+T cells when combined with RT. CD8+T cells were critical to the therapeutic interaction of local tumor RT and systemic AZD0156 administration. In mice with multiple tumors, the combination of RT to one tumor site and systemic AZD0156 administration was not effective in stimulating response at a distant non-radiated tumor site, and we did not detect an increase in tumor infiltrating CD8+T cells at this site following this treatment. This could suggest a translational opportunity and need to consider a combined modality approach that uses a targeted radionuclide therapy in conjunction with an ATM inhibitor to more effectively treat and immunomodulate the tumor microenvironment in settings of metastatic disease. Intriguingly, in mice with multiple tumors, a combination of single tumor RT with systemic AZD0156 administration showed significantly increased CD69 expression in CD8+T cells in non-radiated distant tumors, suggesting a modest immune stimulatory effect of this combined treatment that could be leveraged to enhance systemic antitumor immunity when further combined with immunotherapies, as we observed with anti-PD-L1 therapy.

We have investigated the mechanisms whereby RT and ATM inhibition enhance tumor infiltration by and activation of CD8+T cells. Although RT+AZD0156 showed no effect on tumor infiltration by CD4+T cells or NK cells in the MOC2 tumor model, the B78 tumor model exhibited increased infiltration of CD4+ and CD8+ T cells and NK cells. A previous study using an ATM-deficient B16 murine melanoma model demonstrated a marked effect of ATM-deficiency on tumor infiltration by CD8, CD4, and NK cells.[23] This difference may be due in part to the
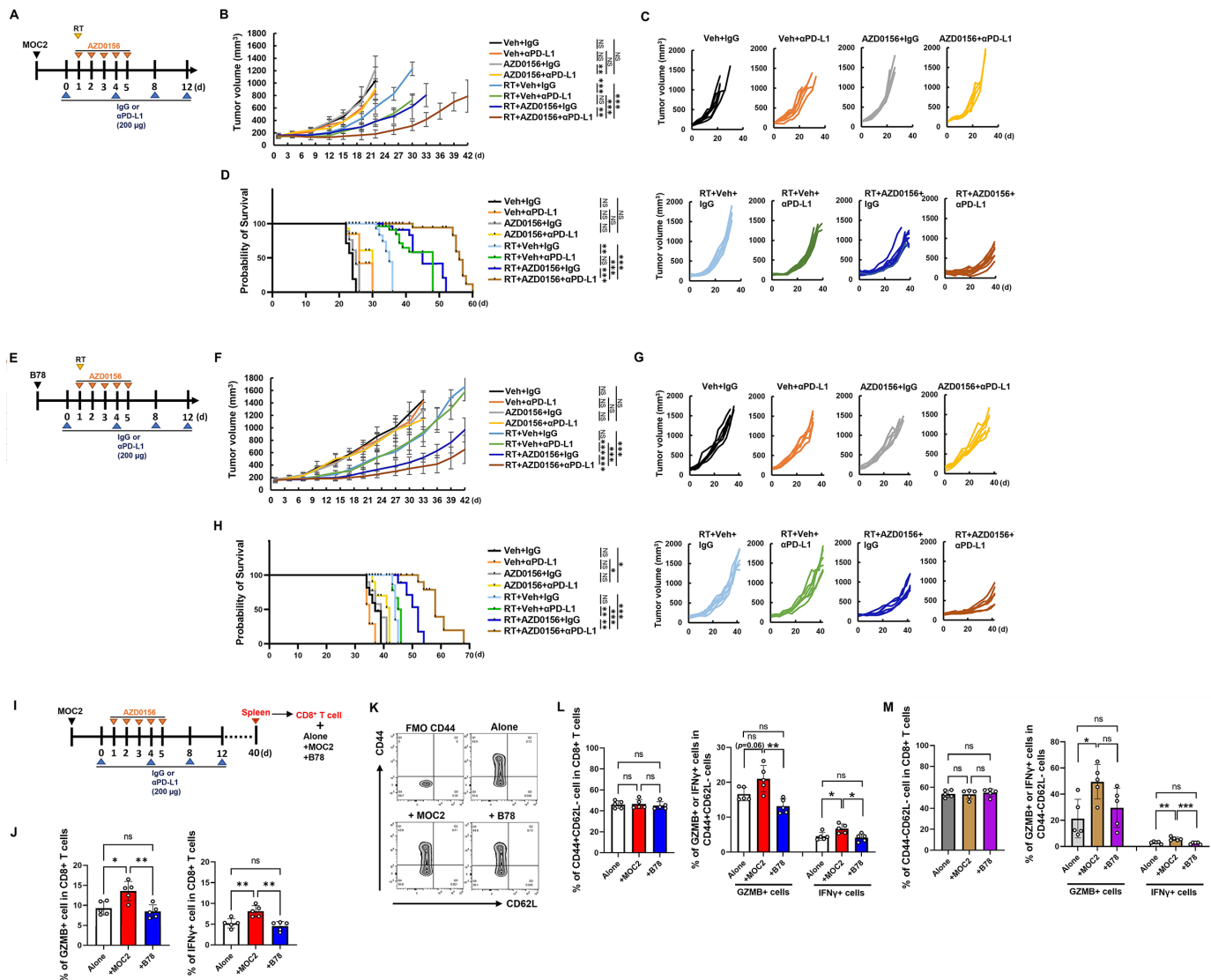
Figure 7 Combining RT+AZD0156 with anti-PD-L1 therapy promotes antitumor immune responses. (A–G) C57BL/6 mice were engrafted subcutaneously with MOC2 or B78 (2×10^6) cells in the right flank. When the mean tumor volume reached 150–200 mm³, the mice were randomized and treated with local tumor RT (0 or 8 Gy for MOC2, and 0 or 12 Gy for B78) 1 hour after oral administration of AZD0156 (200 µg) or vehicle control (oil). The mice were further treated with AZD0156, oil, intraperitoneal IgG or anti-PD-L1 (clone B7-H1, 200 µg) antibody as indicated. (A and E) Treatment regimen, (B and F) tumor growth curves, (C and G) individual tumor volume curves, and (D and H) mouse survival data are shown. (n=6–10/group) (I–M) Spleens were collected on day 40 after indicated treatment in MOC2. (I) Single cell suspension of sorted CD8+T cells were cultured alone or co-cultured with pre-plated MOC2 or B78h. After 24 hours, the cells were collected and analyzed by flow cytometry to determine GZMB-positive or IFN-γ-positive cells in (J) total CD8+T cells, (K and L) CD44+CD62L– cells, or (M) CD44– CD62L– cells. (n=5/group). Significance was determined by linear mixed-effects analysis with Tukey's multiple comparisons (B and F) log-rank testing (D and H) and one-way analysis of variance with post hoc Tukey's (J) L and (M). Veh, vehicle. ns, not significant; *p≤0.05; **p≤0.01; ***p≤0.001. FMO, fluorescence minus one; GZMB, granzyme B; IFN, interferon; PD-L1, programmed death-ligand 1; RT, radiation therapy

use of a different tumor model from ours, the timing or duration of ATM inhibition as compared with constitutive deficiency, or a difference related to the use of RT in our combination treatment approach. Overall, our report and prior studies suggest a potentially critical role for CD8+T cells in the antitumor response to ATM inhibition in radiated tumors. In addition, the antitumor effect that oral administration of ATM inhibitor had in combination with RT provides insight into what drug mechanisms

might best be combined with radiation to enhance its effectiveness.

Although low concentrations of AZD0156 alone did not stimulate an IFN-I response in tumor cells, we observed that the combination of RT+AZD0156 significantly increased the IFN-I response compared with RT alone in both the MOC2 and B78 tumor models. A previous report demonstrated that tumor-derived IFN-I leads to IFNAR1-expressing host immune cell recruitment to the

tumor microenvironment.[53] Consistently, we observed that in mice whose T cells lack IFNAR1, the combination of RT+AZD0156 does not lead to increased tumor infiltration by CD8+T cells. These results suggest that tumor-derived IFN-I signaling is stimulated by the combination of RT+AZD0156 and that IFN-β is a major driver of increased tumor infiltration by CD8+T cells. We further observed that IFN-β signaling in tumors following RT+AZD0156 is dependent on tumor cell expression of STING in the B78 melanoma and MOC2 HNSCC model. More importantly, we report that STING-deficiency reduces chemokine expression in tumors and STING-mediated IFN-β drives cell-autonomous regulation of PD-L1 and MHC-I expression.[54–56] This provides rationale for evaluating anti-PD-L1 therapy in combination with RT+AZD0156 and suggests important translational opportunities for future studies that combine a form of RT, ATM inhibition, or potentially other DNA damage repair pathway inhibition, and anti-PD-L1 immune checkpoint inhibition.

This study has several limitations. We used only a single dose of RT (8 Gy for MOC2 and 12 Gy for B78), which we previously optimized as effective doses in these models for activating an IFN-I response and enhancing antitumor immune response.[11 35] In future studies, it will be valuable to further evaluate the immunologic effects of ATM inhibition in combination with various doses of radiation and with various forms of RT including brachytherapy and targeted radionuclide therapies. In addition, our studies present an initial evaluation of the immunologic effects of RT in combination with ATM inhibition in transplantable syngeneic tumor models. These studies will benefit from further validation in genetically engineered tumor models and/or companion canines with tumors in order to better assess these effects in the setting of tumors that more closely reflect the complexities and immune editing that occurs in the tumors of patients with cancer. Similarly, our findings with AZD0156 are specific to this agent, but further studies are now warranted to better evaluate the generalizability of our observations to the settings of other agents targeting ATM or potentially other components of DDR. While we demonstrate that therapeutic outcomes are improved with the combination of RT+AZD0156 and anti-PD-L1, most mice still succumb to disease. In future studies it will be valuable to further optimize the dosing and timing of these therapies and to investigate the effects of RT+AZD0156 on the expression of additional immune checkpoint ligands that may blunt the durability of antitumor immune response and contribute to immune exhaustion.

Overall, our data provide novel insight on the mechanisms whereby ATM inhibition may be combined with RT to favorably immunomodulate the tumor microenvironment, augment antitumor immunity, and enhance tumor response—either alone or in combination with immune checkpoint blockade. These findings provide rationale for further preclinical and translational studies evaluating the generalizability of these observations with other approaches to DNA damage repair inhibition/ modification and in conjunction with other immunotherapies. Translational studies are warranted to begin exploring the therapeutic potential of combining RT+ATM inhibition+anti-PD-L1 or anti-PD-1 therapy.

Patient consent for publication Not applicable.

Ethics approval Not applicable.

Provenance and peer review Not commissioned; externally peer reviewed.

Data availability statement Data are available upon reasonable request. All data, code, and material generated in this study are available upon request from the corresponding author.

ORCID iDs
Won Jong Jin http://orcid.org/0000-0003-4147-9735
Zachary S Morris http://orcid.org/0000-0001-5558-3547

REFERENCES

1 Demaria S, Bhardwaj N, McBride WH, *et al*. Combining radiotherapy and Immunotherapy: a revived partnership. *Int J Radiat Oncol Biol Phys* 2005;63:655–66.
2 Burnette BC, Liang H, Lee Y, *et al*. The efficacy of radiotherapy relies upon induction of type I interferon-dependent innate and adaptive immunity. *Cancer Res* 2011;71:2488–96.
3 Kedor C, Listing J, Zernicke J, *et al*. Canakinumab for treatment of adult-onset still's disease to achieve reduction of Arthritic manifestation (CONSIDER): phase II, randomised, double-blind, placebo-controlled, Multicentre, investigator-initiated trial. *Ann Rheum Dis* 2020;79:1090–7.
4 Deng L, Liang H, Xu M, *et al*. STING-dependent cytosolic DNA sensing promotes radiation-induced type I interferon-dependent antitumor immunity in Immunogenic tumors. *Immunity* 2014;41:843–52.
5 Trinchieri G. Type I interferon: friend or foe *J Exp Med* 2010;207:2053–63.
6 Formenti SC, Rudqvist N-P, Golden E, *et al*. Radiotherapy induces responses of lung cancer to CTLA-4 blockade. *Nat Med* 2018;24:1845–51.
7 Twyman-Saint Victor C, Rech AJ, Maity A, *et al*. Radiation and dual Checkpoint blockade activate non-redundant immune mechanisms in cancer. *Nature* 2015;520:373–7.

8   Sharabi AB, Nirschl CJ, Kochel CM, *et al*. Stereotactic radiation therapy augments antigen-specific PD-1-mediated antitumor immune responses via cross-presentation of tumor antigen. *Cancer Immunol Res* 2015;3:345–55.

9   Dewan MZ, Galloway AE, Kawashima N, *et al*. Fractionated but not single-dose radiotherapy induces an immune-mediated Abscopal effect when combined with anti-CTLA-4 antibody. *Clin Cancer Res* 2009;15:5379–88.

10 Jagodinsky JC, Jin WJ, Bates AM, *et al*. Temporal analysis of type 1 interferon activation in tumor cells following external beam radiotherapy or targeted radionuclide therapy. *Theranostics* 2021;11:6120–37.

11 Jin WJ, Erbe AK, Schwarz CN, *et al*. Tumor-specific antibody, Cetuximab, enhances the in situ vaccine effect of radiation in Immunologically cold head and neck squamous cell carcinoma. *Front Immunol* 2020;11:591139.

12 Pieper AA, Rakhmilevich AL, Spiegelman DV, *et al*. Combination of radiation therapy, Bempegaldesleukin, and Checkpoint blockade Eradicates advanced solid tumors and metastases in mice. *J Immunother Cancer* 2021;9:e002715.

13 McBride S, Sherman E, Tsai CJ, *et al*. Randomized phase II trial of Nivolumab with stereotactic body radiotherapy versus Nivolumab alone in metastatic head and neck squamous cell carcinoma. *J Clin Oncol* 2021;39:30–7.

14 Theelen WSME, Peulen HMU, Lalezari F, *et al*. Effect of Pembrolizumab after stereotactic body radiotherapy vs Pembrolizumab alone on tumor response in patients with advanced non-small cell lung cancer: results of the PEMBRO-RT phase 2 randomized clinical trial. *JAMA Oncol* 2019;5:1276–82.

15 Lindahl T. Instability and decay of the primary structure of DNA. *Nature* 1993;362:709–15.

16 Jackson SP, Bartek J. The DNA-damage response in human biology and disease. *Nature* 2009;461:1071–8.

17 Ciccia A, Elledge SJ. The DNA damage response: making it safe to play with knives. *Mol Cell* 2010;40:179–204.

18 Burma S, Chen BP, Murphy M, *et al*. ATM Phosphorylates Histone H2Ax in response to DNA double-strand breaks. *J Biol Chem* 2001;276:42462–7.

19 Bartkova J, Horejsí Z, Koed K, *et al*. DNA damage response as a candidate anti-cancer barrier in early human tumorigenesis. *Nature* 2005;434:864–70.

20 Huang RX, Zhou PK. DNA damage response signaling pathways and targets for radiotherapy sensitization in cancer. *Signal Transduct Target Ther* 2020;5:60.

21 Riches LC, Trinidad AG, Hughes G, *et al*. Pharmacology of the ATM inhibitor Azd0156: potentiation of irradiation and Olaparib responses Preclinically. *Mol Cancer Ther* 2020;19:13–25.

22 Zhang Q, Green MD, Lang X, *et al*. Inhibition of ATM increases interferon signaling and sensitizes Pancreatic cancer to immune Checkpoint blockade therapy. *Cancer Res* 2019;79:3940–51.

23 Hu M, Zhou M, Bao X, *et al*. ATM inhibition enhances cancer Immunotherapy by promoting mtDNA leakage and cGAS/STING activation. *J Clin Invest* 2021;131:e139333.

24 Chiu L-Y, Sun Q, Zenke FT, *et al*. Selective ATM inhibition augments radiation-induced inflammatory signaling and cancer cell death. *Aging (Albany NY)* 2023;15:492–512.

25 Gao Y, Li Y, Lin Z, *et al*. Ataxia telangiectasia Mutated kinase inhibition promotes irradiation-induced PD-L1 expression in tumour-associated Macrophages through IFN-I/JAK signalling pathway. *Immunology* 2023;168:346–61.

26 Judd NP, Allen CT, Winkler AE, *et al*. Comparative analysis of tumor-infiltrating lymphocytes in a Syngeneic mouse model of oral cancer. *Otolaryngol Head Neck Surg* 2012;147:493–500.

27 Zolkind P, Przybylski D, Marjanovic N, *et al*. Cancer Immunogenomic approach to Neoantigen discovery in a Checkpoint blockade responsive murine model of oral cavity squamous cell carcinoma. *Oncotarget* 2018;9:4109–19.

28 Becker JC, Varki N, Gillies SD, *et al*. An antibody-interleukin 2 fusion protein overcomes tumor heterogeneity by induction of a cellular immune response. *Proc Natl Acad Sci U S A* 1996;93:7826–31.

29 Uphoff CC, Drexler HG. Detection of Mycoplasma contamination in cell cultures. *Curr Protoc Mol Biol* 2014;106:28.

30 Patel RB, Hernandez R, Carlson P, *et al*. Low-dose targeted radionuclide therapy renders Immunologically cold tumors responsive to immune Checkpoint blockade. *Sci Transl Med* 2021;13:eabb3631.

31 Livak KJ, Schmittgen TD. Analysis of relative gene expression data using real-time quantitative PCR and the 2(-Delta Delta C(T)) method. *Methods* 2001;25:402–8.

32 Bates D, Machler M, Bolker BM, *et al*. Fitting linear mixed-effects models using Lme4. *J Stat Softw* 2015;67:1–48.

33 Kuznetsova A, Brockhoff PB, Christensen RHB. lmerTest package: tests in linear mixed effects models . *J Stat Soft* 2017;82:1–26.

34 Lim JYH, Gerber SA, Murphy SP, *et al*. Type I Interferons induced by radiation therapy mediate recruitment and Effector function of Cd8(+) T cells. *Cancer Immunol Immunother* 2014;63:259–71.

35 Morris ZS, Guy EI, Francis DM, *et al*. In situ tumor vaccination by combining local radiation and tumor-specific antibody or Immunocytokine treatments. *Cancer Res* 2016;76:3929–41.

36 Obst R. The timing of T cell priming and Cycling. *Front Immunol* 2015;6:563.

37 Lu C, Klement JD, Ibrahim ML, *et al*. Type I interferon suppresses tumor growth through activating the Stat3-Granzyme B pathway in tumor-infiltrating cytotoxic T lymphocytes. *J Immunother Cancer* 2019;7:157.

38 Shiow LR, Rosen DB, Brdicková N, *et al*. Cd69 acts downstream of interferon-alpha/beta to inhibit S1P1 and lymphocyte egress from Lymphoid organs. *Nature* 2006;440:540–4.

39 Morimoto Y, Kishida T, Kotani S-I, *et al*. Interferon-B signal may up-regulate PD-L1 expression through Irf9-dependent and independent pathways in lung cancer cells. *Biochem Biophys Res Commun* 2018;507:330–6.

40 Garcia-Diaz A, Shin DS, Moreno BH, *et al*. Interferon receptor signaling pathways regulating PD-L1 and PD-L2 expression. *Cell Rep* 2019;29:3766.

41 Wan S, Pestka S, Jubin RG, *et al*. Chemotherapeutics and radiation stimulate MHC class I expression through elevated interferon-beta signaling in breast cancer cells. *PLoS One* 2012;7:e32542.

42 Reits EA, Hodge JW, Herberts CA, *et al*. Radiation modulates the peptide repertoire, enhances MHC class I expression, and induces successful antitumor Immunotherapy. *J Exp Med* 2006;203:1259–71.

43 Wu CT, Chen WC, Chang YH, *et al*. The role of PD-L1 in the radiation response and clinical outcome for bladder cancer. *Sci Rep* 2016;6.

44 Baird JR, Friedman D, Cottam B, *et al*. Radiotherapy combined with novel STING-targeting Oligonucleotides results in regression of established tumors. *Cancer Res* 2016;76:50–61.

45 Zebertavage LK, Alice A, Crittenden MR, *et al*. Transcriptional upregulation of Nlrc5 by radiation drives STING- and interferon-independent MHC-I expression on cancer cells and T cell cytotoxicity. *Sci Rep* 2020;10:7376.

46 Nakano M, Fujii T, Hashimoto M, *et al*. Type I interferon induces Cx3Cl1 (Fractalkine) and Ccl5 (RANTES) production in human pulmonary vascular endothelial cells. *Clin Exp Immunol* 2012;170:94–100.

47 Antonelli A, Ferrari SM, Fallahi P, *et al*. Interferon-alpha, -Beta and -Gamma induce Cxcl9 and Cxcl10 secretion by human Thyrocytes: modulation by peroxisome Proliferator-activated receptor-gamma agonists. *Cytokine* 2010;50:260–7.

48 Kohli K, Pillarisetty VG, Kim TS. Key Chemokines direct migration of immune cells in solid tumors. *Cancer Gene Ther* 2022;29:10–21.

49 Chew V, Chen J, Lee D, *et al*. Chemokine-driven lymphocyte infiltration: an early Intratumoural event determining long-term survival in Resectable hepatocellular carcinoma. *Gut* 2012;61:427–38.

50 Nolz JC, Starbeck-Miller GR, Harty JT. Naive, Effector and memory Cd8 T-cell trafficking: parallels and distinctions. *Immunotherapy* 2011;3:1223–33.

51 Nakajima Y, Chamoto K, Oura T, *et al*. Critical role of the Cd44(Low) Cd62L(Low) Cd8(+) T cell subset in restoring antitumor immunity in aged mice. *Proc Natl Acad Sci U S A* 2021;118.

52 Li Y, Yang DQ. The ATM inhibitor KU-55933 suppresses cell proliferation and induces apoptosis by blocking AKT in cancer cells with Overactivated AKT. *Mol Cancer Ther* 2010;9:113–25.

53 Zitvogel L, Galluzzi L, Kepp O, *et al*. Type I Interferons in anticancer immunity. *Nat Rev Immunol* 2015;15:405–14.

54 Gato-Cañas M, Zuazo M, Arasanz H, *et al*. Pdl1 signals through conserved sequence motifs to overcome interferon-mediated cytotoxicity. *Cell Rep* 2017;20:1818–29.

55 Bander NH, Yao D, Liu H, *et al*. MHC class I and II expression in prostate carcinoma and modulation by interferon-alpha and -Gamma. *Prostate* 1997;33:233–9.

56 Zanon RG, Cartarozzi LP, Victório SCS, *et al*. Interferon (IFN) beta treatment induces major Histocompatibility complex (MHC) class I expression in the spinal cord and enhances axonal growth and motor function recovery following Sciatic nerve crush in mice. *Neuropathol Appl Neurobiol* 2010;36:515–34.